

# EllipSect: A Surface Brightness Analysis Tool for GALFIT 3

C. Añorve <sup>1</sup>, O. U. Reyes-Amador <sup>2</sup>, E. Ríos-López <sup>3,4,5</sup>, D. de Ramón Tadeo<sup>6</sup> and O. López-Cruz <sup>3</sup>

<sup>1</sup>Facultad de Ciencias de la Tierra y el Espacio, Universidad Autónoma de Sinaloa, Blvd. de la Américas y Av. Universidad s/n, Ciudad Universitaria, Culiacán, Sinaloa, 80013, México.

<sup>2</sup>Instituto de Radioastronomía y Astrofísica, UNAM, Campus Morelia, AP 3-72, C.P. 58089, México.

<sup>3</sup>Instituto Nacional de Astrofísica, Óptica y Electrónica (INAOE), Luis Enrique Erro 1, Apartado Postal 51 y 216, C.P. 72840 Puebla, México.

<sup>4</sup>Instituto de Astrofísica de Canarias (IAC), Vía Láctea s/n, 38205, La Laguna, Tenerife, España.

<sup>5</sup>Universidad Pedagógica del Estado de Sinaloa, Castiza s/n, 80027, Culiacán, Sinaloa, México.

<sup>6</sup>Facultad de Ciencias de la Computación, Benemérita Universidad Autónoma de Puebla (FCC-BUAP), Av. San Claudio y 14 Sur, Ciudad Universitaria, C.P. 72570, Puebla, México.

**Keywords:** *galaxies: photometry, galaxies: fundamental parameters, methods: data analysis*

## Abstract

EllipSect is a user-friendly analysis and measurement tool, implemented in Python, that operates on the imaging data together with the output of the widely used 2D surface-brightness fitting code GALFIT 3. It produces publication-quality figures and exportable data products to enable quantitative assessment of GALFIT 3 models and their individual components. In addition, EllipSect computes non-parametric measurements that are not provided by GALFIT 3, including the total effective radius resulting from multi-component fits, cusp radius, and the Petrosian radius. This paper provides examples and a quick guide for EllipSect.

## Resumen

EllipSect es una herramienta de análisis y medición, implementada en Python, que opera sobre los datos de imagen junto con la salida del código ampliamente utilizado de ajuste bidimensional de brillo superficial GALFIT 3. Genera figuras de calidad publicable y productos de datos exportables para permitir una evaluación cuantitativa de los modelos de GALFIT 3 y de sus componentes individuales. Además, EllipSect calcula mediciones no paramétricas que no son proporcionadas por GALFIT 3, incluyendo el radio efectivo total resultante de ajustes multicomponente, el radio de cúspide y el radio de Petrosian. Este artículo presenta ejemplos y una guía rápida de uso de EllipSect.

**Corresponding author:** Christopher Añorve *E-mail address:* [canorve@uas.edu.mx](mailto:canorve@uas.edu.mx)

## 1. Introduction

GALFIT 3<sup>1</sup> (Peng et al., 2002, 2010) is a widely used stand-alone two-dimensional (2D) fitting code designed to model the surface brightness (SB) distribution of astronomical sources by generating 2D-parametric models that account for galaxies' substructures and individual stars, among others. With GALFIT 3, the user can apply multiple profiles to fit the following components: bulges, disks, bars, spiral arms, and asymmetries to one or several galaxies simultaneously.

Furthermore, when dealing with multiple components, the orientation of each component is independent of the others; hence, component-based separation is more reliable. This property gives a substantial advantage in crowded galaxy fields, such as compact groups or clusters of galaxies. Indeed, our experience shows that masking does not adequately account for light from nearby or overlapping galaxies; instead, fitting

the galaxy of interest along with its neighboring galaxies yields a better result. Indeed, Häussler et al. (2007); Añorve (2012) tested this recommendation using simulated data and found that fitting neighboring galaxies simultaneously accounts for galaxies' extended light more precisely.

Another feature of GALFIT 3 is that a user-supplied point spread function (PSF) image is necessary, or the user may utilize the built-in functions provided by GALFIT 3 to model the PSF. GALFIT 3 convolves the PSF with the chosen profile to fit a given galaxy. This differs from some previous methods, which relied on deconvolving the image (for example Lucy, 1974; Richardson, 1972) before generating isophotes (e.g., Jedrzejewski, 1987) and fitting the SB profile.

GALFIT 3 applies a  $\chi^2$  optimization scheme for parameter selection, including the background, generating parameter uncertainties, and producing a FITS (Flexible Image Transport System) image cube containing the image of the input object, the model image resulting after the fit, and the residual image. However, GALFIT 3 does not include a graphical tool to compare

<sup>1</sup>For installation, usage, and general help, visit <https://users.obs.carnegiescience.edu/peng/work/galfit/galfit.html>

the input image with its resulting model image. Users commonly applied one-dimensional (1D) IRAF’s `ellipse` and other plotting programs; nevertheless, this suite of programs became difficult to access after IRAF’s discontinuation in 2013. Fortunately, IRAF’s `ellipse` is implemented in the Astropy library and is available in new releases. In any case, the main difficulty is that one must convert GALFIT 3’s output format to a format accepted by external codes. Nevertheless, this process could be time-consuming and error-prone. However, this method is not feasible with IRAF’s `ellipse` task, which processes only one galaxy at a time. Also, a common misconception suggests that 1D approaches work better in low signal-to-noise (S/N) regions or the presence of low-SB features; however, there is no advantage from 1D over the 2D approaches due to the Poissonian nature of the signal<sup>2</sup> (see also Press et al., 2007; Peng et al., 2010).

Hence, we are introducing EllipSect, a new algorithm that generates SB profiles and extracts complementary information directly from GALFIT 3’s output, with the current implementation coded in Python. The current manuscript focuses on EllipSect as a post-fit analysis tool that produces quantitative measurements, publication-quality graphics, and exportable data products from the observed galaxy and GALFIT 3 models. These products can also support iterative model refinement (e.g., adding or removing components) when needed. EllipSect’s output includes data from the observed galaxy, and its model fits in the form of one-dimensional profiles. For a more straightforward assessment of the results, EllipSect can handle individual model components for a detailed analysis.

Additionally, EllipSect provides non-parametric measurements derived from the data and the GALFIT 3 model/output, such as integrated magnitudes, mean SB at  $r_e$  ( $\langle\mu\rangle_e$ ), the SB at  $r_e$  ( $\mu_e$ ), the radius at 90% of total light, Kron radius (Kron, 1980), Petrosian radius (Petrosian, 1976), bulge-to-total ratio, and the total effective radius ( $r_e'$ ) of a galaxy with multiple components fits.

To make this paper self-contained, Appendix A provides a brief history, applications, and analytical profiles implemented in GALFIT 3. We intended to order them logically, from the more general instance through their particular cases, to avoid the impression that the suite of profiles included in GALFIT 3 is merely a simple list of unrelated profiles.

This paper contains the following sections: §1 presents a general introduction to GALFIT 3 and the built-in profiles; §2 explains EllipSect’s implemented algorithms. §3 shows applications and examples, §4 and §5 presents a discussion and conclusions, respectively. The appendices show the build-up of the GALFIT 3 functions and explain how to install and run EllipSect.

## 2. EllipSect

This section explains how EllipSect works. We have divided it into two parts: first, we describe the main algorithm, and then, we explain the photometric measurements. Throughout this article, we refer to the individual profiles that comprise a SB model as the components. In contrast, the set of SB components constitutes the *model*.

### 2.1. The Algorithm

EllipSect was designed to be user-friendly for most users. It omits any direct interaction with the code or translation of GALFIT

3’s data format. EllipSect is executed from the command line. It requires only the latest GALFIT 3 model output files.

GALFIT 3’s output files consist of a data cube in FITS format, which includes the original image (chopped into the fit region), the model image, and the residual image (i.e., galaxy image – model image), as well as a file named `galfit.nn` (where `nn` indicates the number of attempts run by GALFIT 3). This last file contains the parameters that fit each component of the model. Additionally, GALFIT 3 creates a log file that includes the model parameter values and their associated errors. EllipSect uses the GALFIT output file (`galfit.nn`) to parse the input magnitude zero point, plate scale, mask file name, output file, and model parameters.

The output GALFIT 3 file may include information about the simultaneous fits of neighboring galaxies to the target galaxy. Using the distances among the model components, EllipSect can identify the elements associated with each galaxy.

EllipSect uses the same mask employed by GALFIT to remove the undesired pixels from the image. Once this is done, EllipSect reads the sky component from the GALFIT output file and subtracts it from the output galaxy and model images. The program divides the galaxy and its model into sectors equally spaced in angle around their centers, using the `sectors_photometry` routine from the `mgefit`<sup>3</sup> Python library by Cappellari (2002). With this routine, EllipSect employs these sectors to compute the surface brightness at multiple radii. It divides an ellipse, centered on the galaxy, into multiple sectors according to the geometric information from the GALFIT 3 output file until reaching a minimum count level, set by the `MINLEVEL` parameter, and its preselected value is zero. EllipSect takes the angular orientation and ellipticity from the last component of the GALFIT 3 output file (see B.2) as default values. This component is typically an exponential model, although this may vary with the specific galaxy model employed. The user can change all default parameters.

EllipSect generates publication-quality graphs. It produces two basic graphs in its simplest mode: one showing the averaged surface brightness along the major axis and another displaying the SB for various azimuthal angles across multiple plots (see examples in the Results section). Additionally, this mode generates a `png` image featuring the galaxy, model, and residual. EllipSect can also export a file containing the data points for each plot, allowing users to create custom visualizations with other plotting routines. Optionally, the SB profile for each plot component can include the galaxy (via the `-comp` flag). This feature allows users to visualize the behavior of model components and identify irrelevant components or redundancies (see, for example, Figure 3).

According to the `mgefit` manual, the SB results from the following expression<sup>4</sup>:

$$\mu_l = zpt + 5 \times \log(Pl_{scc}) + 2.5 \times \log(t_{exp}) - 2.5 \times \log(C_0) + 0.1, \quad (1)$$

where  $zpt$  is the magnitude zero point,  $C_0$  are the  $counts \times pixel^{-1}$ ,  $Pl_{scc}$  is the plate scale,  $t_{exp}$  is the exposition time, and 0.1 is a correction for infinite aperture.

<sup>2</sup>See a more detailed discussion at <https://users.obs.carnegiescience.edu/peng/work/galfit/TFAQ.html#misconception1> on 1D vs. 2D modeling

<sup>3</sup>`mgefit` is a software to obtain Multi-Gaussian Expansion (MGE) fits of galaxy images (Cappellari, 2002)

<sup>4</sup>This does not include the extinction parameter

## 2.2. Output photometry

In addition to generating surface brightness plots, EllipSect calculates additional photometric variables from the models beyond those provided by GALFIT 3. These variables are stored in an output file and are computed after EllipSect extracts the counts for each sector. This section describes these variables and explains how they are calculated.

EllipSect connects to NED through the command `curl` to download an xml file to extract the photometric corrections and compute the absolute magnitude according to the appropriate band. To transform magnitudes to luminosities, and vice-versa, the absolute magnitude of the Sun from Willmer (2018) is assumed. This file extracts the distance modulus and the galactic extinction (Schlafly & Finkbeiner, 2011). It also retrieves a conversion parameter used to convert angular units to Kpc. SB dimming also corrects the mean SB at effective radius  $\langle \mu \rangle_e$  and SB at the effective radius  $\mu_e$ . The only correction not applied is the k-correction, as it needs the color information that is not always available (e.g., see Chilingarian & Zolotukhin, 2012). It is important to note that corrections are applied only to the quantities in the output file, while the single and multiple plots mentioned earlier do not include these corrections. However, users can apply a correction factor either as a command-line argument or by generating plots from the EllipSect output files.

NED provides two distance-modulus measurements: one derived from cosmological models and the other obtained directly from the galaxy. By default, EllipSect uses the redshift-independent measurement to calculate the luminosity, if available. Otherwise, it uses the distance modulus based on cosmological models.

The majority of photometric parameters are calculated within an ellipse that encloses 90% of the total light. Some of those associated photometric parameters are the Bumpiness (Blakeslee et al., 2006), the Tidal parameter (Tal et al., 2009), the reduced chi-squared ( $\chi^2_\nu$ ) within this ellipse (as opposed to the value provided by GALFIT 3, which applies to the entire fitted image section), the signal-to-noise ratio (S/N), the residual sum of squares, the number of degrees of freedom, the number of free parameters, the absolute magnitude, the bulge-to-total ratio, and the luminosity.

The Bumpiness parameter quantifies the irregular structure of a galaxy by measuring deviations in its SB from a smooth SB model. Blakeslee et al. (2006) employed this parameter and the Sérsic index to classify galaxies into elliptical, S0, spiral, and irregular types.

The calculation of the Bumpiness  $B$  results from the following formula:

$$B = \frac{\left( \frac{1}{N} \sum_{r_{i,j} < 2r_e} [I_{i,j} - S(x_i, y_j | r_e, n)]_s^2 - \sigma_s^2 \right)^{\frac{1}{2}}}{\frac{1}{N} \sum_{r_{i,j} < 2r_e} S(x_i, y_j | r_e, n)}, \quad (2)$$

The sum extends over two effective radii ( $2r_e$ ), but in this case, the sum is taken within the region of the ellipse defined above. Here,  $N$  represents the number of unmasked pixels included in the computation,  $I_{i,j}$  is the galaxy intensity at pixel  $(i, j)$ ,  $S$  is the convolved surface brightness model, and  $\sigma_s^2$  is the estimated photometric error, which is taken directly from the sigma image produced by GALFIT 3.

Another useful parameter is the Tidal parameter, defined as:

$$T_{gal} = \left[ \left( \frac{I_{(x,y)}}{M_{(x,y)}} \right) - 1 \right], \quad (3)$$

where  $I_{(x,y)}$  are the galaxy pixel intensity values in  $(x, y)$  and  $M_{(x,y)}$  represent the intensity values of the model.

This parameter measures the differences between the galaxy image and its corresponding model. Tal et al. (2009) used this to measure the tidal disturbances in elliptical galaxies and explored their relation with environmental properties, AGN activity, and color.

EllipSect is particularly useful to determine the total effective radius,  $r_e^t$ , of a galaxy when its SB model results after a multicomponent fit, for example, for a fit including a bulge, a disk, and a bar (Sérsic+Exponential+Sérsic), while GALFIT 3 only generates  $r_e$  for each component; EllipSect calculates the total effective radius by summing all subcomponents of the galaxy's SB model, calculating half of the total flux, and finding the corresponding radius using the bisection method. In the manual of GALFIT 3, the author suggests the application of a single Sérsic fit for the entire galaxy, using  $r_e$  from the GALFIT 3 fit as a proxy for  $r_e^t$ . We argue that EllipSect significantly extends this approximation.

To resolve this, EllipSect employs a numerical method that adds together the models of all components and then locates the radius where the total luminosity reaches half of its overall value ( $r_e^t$ ). This procedure can also be applied to determine the radius corresponding to any percentage of the total light.

EllipSect provides additional ways to determine the goodness of fit by calculating the Akaike Information Criterion (AIC, Akaike, 1974) and the Bayesian Information Criterion (BIC, Schwarz, 1978), which enable to determine the best fit for the galaxy among a given set of models. Both criteria penalize adding new parameters by increasing the estimate of  $\chi_\nu$ . The model with the lowest AIC or BIC value is considered the best fit. EllipSect also computes an alternative BIC using the number of resolution elements instead of the number of pixels defined by  $N_{res} = \frac{n_{pix}}{\pi(\text{FWHM})^2}$ .

Finally, additional output parameters are computed for each model component, including the fraction of light (such as the bulge-to-total ratio for each component),  $\langle \mu \rangle_e$ ,  $\mu_e$ , absolute magnitude, luminosity radius at 90% of the total light, Kron radius (Kron, 1980), and Petrosian radius (Petrosian, 1976). Accurate determination of those parameters requires a precise estimation of the sky background.

### 2.2.1. Sky computation

An incorrect sky background estimation can lead to inaccurate surface brightness model parameters, especially the Sérsic index. An appropriate strategy is to determine and fix the sky background during model fitting, thereby reducing the number of free parameters and preventing parameter degeneracy.

EllipSect provides two methods for computing the sky background: the sky gradient method and the random box method. GALFIT 3 does not include these two methods; therefore, by comparing the results, the user decides whether to retain the model or refine it by using the newly derived sky value from EllipSect.

**Sky gradient method:** This method follows Barden et al. (2012). In this approach, EllipSect constructs concentric rings using the same angular parameters and ellipticity employed for the elliptical sectors described in 2.1. The user specifies the ring width and EllipSect enlarges the rings' major axes outward from the galaxy's center. EllipSect can remove the top 80% and bottom 20% of sky values in each ring; however, the user can also specify a mask file to exclude undesired pixels. Finally,

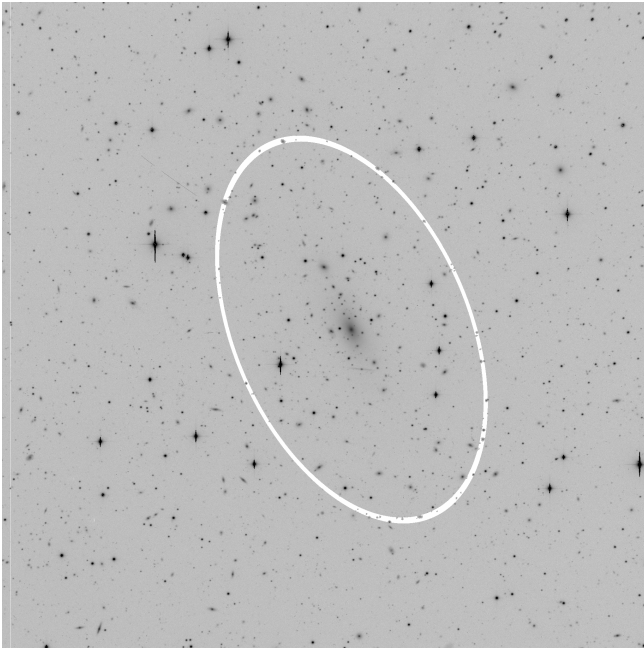


**Figure 1.** Example of sky computation using the gradient method. The ring around the brightest cluster member of Abell 2029 indicates the radius used by EllipSect to compute the sky. For visualization purposes, all pixels in that elliptical ring are assigned the same numerical value corresponding to the ellipse’s major-axis length.

EllipSect computes the gradient from the mean sky values of each ring.

A negative gradient arises in the galaxy’s inner regions because the central counts exceed those in the outskirts. Beyond this zone, the gradient fluctuates randomly between positive and negative values (see Figure 5 in Barden et al. (2012)). EllipSect generates a fit image with sky rings to illustrate this gradient. It begins calculating the gradient from an initial radius and stops when it becomes positive for the second time, following the recommendation by Barden et al. (2012). At that point, EllipSect returns the sky value determined for this radius. Figure 1 shows an example of an elliptical ring used to compute the sky.

**Random box method:** For this method, EllipSect calculates the sky using randomly placed boxes around the galaxy. To achieve this, it first creates an elliptical mask that covers the entire galaxy. By default, the geometry for this elliptical mask comes from the GALFIT 3 output file, although the user may modify it.

Next, the program positions boxes randomly between this elliptical mask and a specified maximum radius (often at the image boundary). It can also optionally remove the top 80% and bottom 20% of pixel values within these boxes. The final sky value is the mean of the median and standard deviation of all pixels within the boxes. The default settings place 20 boxes, each measuring 20 pixels across. This method follows the approach described in Gao & Ho (2017).

### 3. Results: Examples of SB plots

Ríos-López et al. (2021) and Ríos-López et al. (2025) applied EllipSect in their study of Two Micron All Sky Survey (2MASS) galaxies, where they applied GALFIT 3 to generate estimates of morphological and structural parameters through photometric decompositions. In another study by Reyes-Amador (2021),

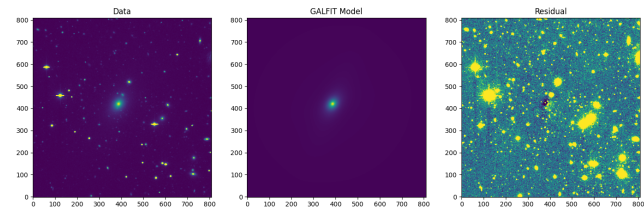


**Figure 2.** Example of cube image generated by EllipSect. The left panel shows the galaxy, the middle panel is the model, and the right panel is the residual. The user can change the color palette, brightness, and contrast.

EllipSect was used to map dust in the cores of local Active Galactic Nuclei (AGN), using Hubble Space Telescope (HST) images, SB models, and radiative transfer simulations. The code has also been used in reports, conference proceedings, professional papers, and undergraduate and graduate theses (e.g., Ríos-López, 2021; Duggal et al., 2024, Valerdi M. et al. 2026, in preparation).

Here, we present examples of SB profiles for three images: Holm 15A from the Kitt Peak National Observatory (KPNO), M61 from 2MASS, and NGC 4261 from the HST.

#### 3.1. Kitt Peak: Holm 15A

This example shows the SB profile plots of the Abell 85 brightest cluster galaxy (BCG), the cD galaxy Holm 15A. Here, GALFIT 3 was used to fit a multi-Gaussian component to model the SB; this result complements the analysis of López-Cruz et al. (2014), who used Nuker profiles. These observations were obtained with the KPNO 0.9m Telescope and are part of the LOCOS catalog (López-Cruz, 1997). The reader can find details on the selection criteria, observations, and data reduction in López-Cruz (1997), López-Cruz et al. (2004), and López-Cruz et al. (2026, in preparation). In Figure 2, we show the cube image generated by EllipSect for this galaxy.

In Figure 3, we present the single-plot of the SB of Holm 15A. Seven Gaussians were used to cover the whole SB profile. The plot also shows the percent error. This figure was generated automatically by EllipSect, which computes the SB profiles of the galaxy, model, and individual components.

#### 3.2. 2MASS: M61

In Figure 4, we show the galaxy, model, and residual for galaxy M 61 in the  $K_s$  band of 2MASS.

Figure 5 shows the multiplot of the fitting of M 61. This model consists of a series of Sérsic and Exponential components. In the region where the model fails to reproduce the SB model of the galaxy, it results in apparent deviations.

#### 3.3. HST: NGC4261

In the last example, we display an HST image of NGC 4261. Figure 6 includes the actual galaxy, its model, and its residual.

Figure 7 shows the galaxy NGC4261 taken with the HST using filter F547M. This model used a single Sérsic component to fit the galaxy’s SB.

## 4. Discussion

EllipSect was developed to generate surface brightness profile plots, calculate non-parametric measurements, and export data derived from GALFIT model outputs. Its primary purpose is to test the reliability of GALFIT 3’s model at various radii and

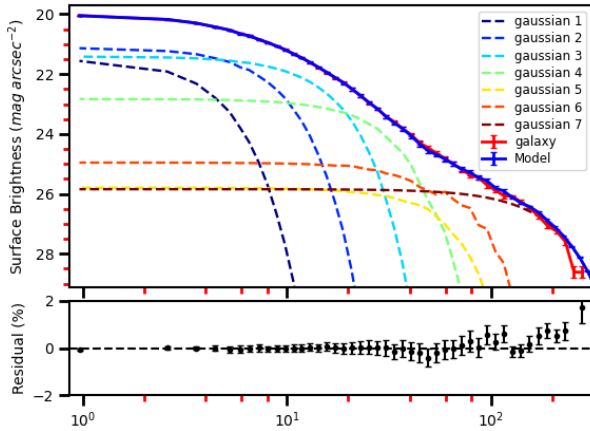


**Figure 3.** Example of EllipSect output for the cD galaxy Holm 15a and its model. It shows a seven-Gaussian component fit. The red continuous line represents the galaxy and the blue continuous line represents the multicomponent GALFIT 3 model. Each Gaussian component is shown as a dashed line and is color-coded, as indicated in the inset box at the top right. The plot shows average SB vs. radius along the major axis. The residual percentage is displayed in the bottom plot.

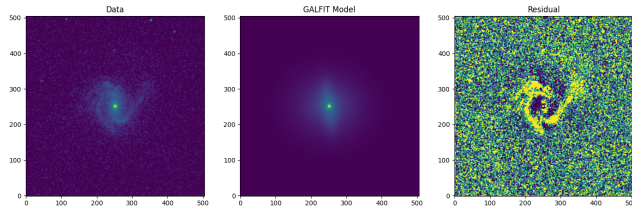


**Figure 4.** Example of cube image generated by EllipSect for M 61 galaxy. Details for this image are the same as the caption of Figure 2.

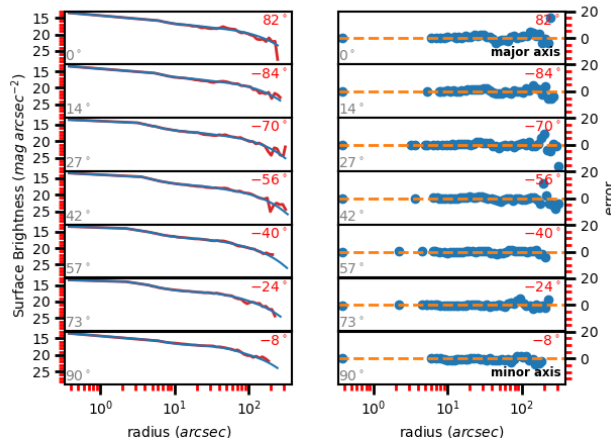


**Figure 5.** Example of EllipSect multi-plot output for M 61 galaxy and its model. This figure shows multiple plots of galaxy SB and model at different angles from the major axis (the major axis is the one with 0 deg). The error is shown on the right hand side of the multiplot. The angle in red at the top right indicates the angle measured relative to the image's Y-axis. On the other hand, the subtle grey angle at the bottom left indicates the angle measured from the major axis, starting from the top, with the major axis and the bottom plot with the minor axis.

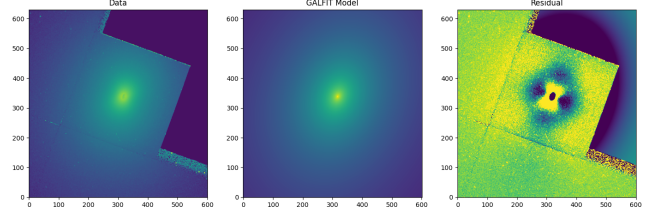


**Figure 6.** Example of cube image generated by EllipSect for NGC4261 galaxy. Details for this image are the same as the caption of Figure 2.

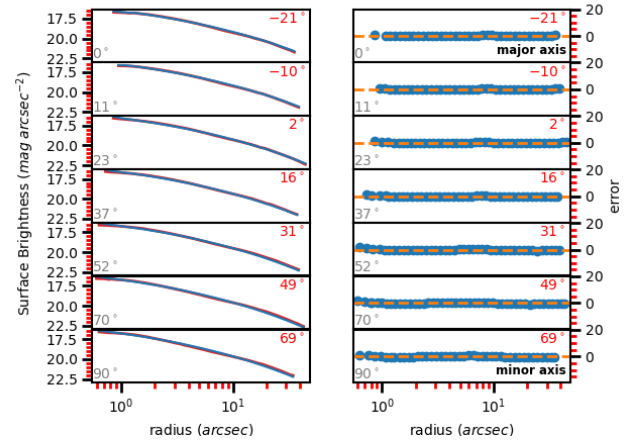


**Figure 7.** Example of EllipSect output for NGC4261 galaxy and its model. The description of the image is the same as Figure 5.

angles for a given galaxy. In addition, EllipSect allows users to include individual components of the GALFIT 3 models in the plots, enabling verification that these components behave as expected. This feature streamlines the analysis process by eliminating the need to switch between different program formats, making it practical to quickly confirm that the GALFIT model is appropriate for the galaxy. EllipSect aids GALFIT 3 users with a readily accessible and easy-to-use tool for generating accurate SB measurements and publication-quality plots.

One typically uses IRAF's `ellipse` in the conventional approach to generating SB profiles. This routine fits an ellipse to each isophote at every radius, from the central region to the galaxy's outskirts. As the radius changes, the ellipse's ellipticity and position angle may also vary.

One caveat of EllipSect is that it maintains the ellipticity and the angular position fixed throughout the entire galaxy, overlooking any possible variations of these parameters with radius. However, this fixed-parameter approach is advantageous when dealing with galaxies fitted simultaneously using GALFIT 3. In such cases, masking or removing the galaxy is insufficient, as the galaxies are blended on the line of sight, and it is challenging to distinguish where one galaxy ends, and the other begins (e.g., Häußler et al., 2007). In addition, EllipSect avoids the need for "double" fitting, i.e., two-dimensional and one-dimensional fitting, which IRAF's `ellipse` requires. One-dimensional routines may not be capable of simultaneous fitting isophotes for two neighboring galaxies, making simultaneous fitting difficult or impossible. While EllipSect is not a complete substitute for IRAF's `ellipse`, it offers alternative techniques to address the

limitations of isophotal fitting.

Despite the widespread use of IRAF’s `ellipse`, alternative techniques such as `EllipSect` offer unique advantages for SB analysis, which may benefit astronomers seeking to enhance their understanding of galactic structures.

The parameter  $r_e^t$  is the effective radius of the entire galaxy, which is an essential parameter derived by `EllipSect`;  $r_e^t$  is critical to assess metallicity gradients, effective velocity dispersion ( $\sigma_{eff}$ ) and other relevant information (e.g., [Garduño et al., 2023](#)) or comparisons with numerical models. However, no single component’s  $r_e$  can accurately describe an entire galaxy, unless we deal with pure disk or bulge galaxies.

Determining which aperture to use for a galaxy’s photometric variables can be somewhat arbitrary. Different photometric quantities require a suitable radius for proper evaluation, and standardizing this across various galaxies is difficult. In the case of GALFIT 3, the reduced chi-squared ( $\chi_v^2$ ) is computed using all pixels within the fitting region. However, changing the size of this region can alter  $\chi_v^2$  and may include pixels from other objects, introducing additional noise. Consequently, the  $\chi_v^2$  reflects the fit quality for every object within that region.

`EllipSect` uses the radius containing 90% of the total light to compute various photometric variables,  $r_{90}$  which is calculated in the same fashion as the effective radius. Considering the region that contains 90% of the total light minimizes the contamination from external objects. `EllipSect` calculates the Tidal parameter, Bumpiness, AIC, BIC, and a local  $\chi_v^2$  inside  $r_{90}$ .

`EllipSect` provides corrections for galactic extinction and surface brightness dimming, but does not perform k-corrections at this time. Users can still apply morphological-based corrections to the galaxy, although this may be imprecise for cluster galaxies whose colors can differ from those of field galaxies. In such situations, manual correction is recommended. There are many ways to generate k-corrections, we found the tool <http://kcor.sai.msu.ru/>, which uses redshift and the color index of a given galaxy as input ([Chilingarian & Zolotukhin, 2012](#)).

`EllipSect` provides a helpful useful tool for wrapping code to automate GALFIT 3 fitting process. It can efficiently compute the necessary photometric variables required by these codes, thereby allowing for rapid analysis of model outputs for multiple galaxies, which would otherwise be time-consuming. In fact, `EllipSect` has been also designed to be used in conjunction with the Driver for GALFIT on Cluster Galaxies (DGCG) code ([Añorve et al., in preparation](#)), which automates GALFIT 3 fitting for galaxies in dense environments.

## 5. Conclusions and Future Work

This paper introduces `EllipSect` algorithm implemented in Python designed to analyze outputs from GALFIT 3. It generates surface brightness profiles for galaxies, models, and individual components, offering single-plot and multiplot visualizations. Additionally, `EllipSect` computes various photometric parameters, including light fractions for each component,  $r_e^t$ ,  $\langle \mu \rangle_e$ ,  $\mu_e$ , absolute magnitudes, the luminosity radius 90%, the effective radius of the galaxy, the Kron radius, and the Petrosian radius. It also calculates Tidal and Bumpiness parameters, signal-to-noise ratios, and local  $\chi_v^2$  values to assess differences between models and observed galaxies.

`EllipSect` offers two methods for computing the sky background and enables users to distinguish among different galaxy models by computing Bayesian information criteria. The

code can be easily adapted to other GALFIT 3 wrapping codes and will be integrated with DGCG in future work. This project aims to apply `EllipSect` to analyze data images containing hundreds of galaxies, such as galaxy clusters.

`EllipSect` is a robust tool for analyzing GALFIT 3 output and extracting extensive photometric information for galaxies. Its flexibility and versatility make it an essential tool for studying galaxy properties and morphology. Future development will focus on expanding its capacity to handle larger datasets and integrate it with other GALFIT 3 wrapping codes.

## ■ APPENDICES

### A. GALFIT 3 built-in functions or profiles

Below, we describe the built-in functions or profiles implemented in the last distribution of GALFIT 3<sup>5</sup>. We cite the original sources and main applications of each profile. [Baes \(2020\)](#) has shown that the Nuker profile is the most general profile, which includes the Sérsic profiles as a special case; hence, we have ordered the profiles from the more general to the particular cases. Our aim in including the profiles in this appendix is to homogenize the notation with that commonly used in textbooks.

1. **Nuker ([Lauer et al., 1995](#))**: This is a general profile that includes three power-law slopes, namely:  $\gamma$  (inner),  $\alpha$  (sharpness of the transition from inner to outer slopes), and  $\beta$  (outer), they are free to vary and help to account for the large cores of very luminous early-type galaxies, including cD galaxies. This profile is expressed as follows:

$$I(r) = I_b 2^{\left(\frac{\beta-\gamma}{\alpha}\right)} \left(\frac{r_b}{r}\right)^\gamma \left[1 + \left(\frac{r}{r_b}\right)^\alpha\right]^{\left(\frac{\gamma-\beta}{\alpha}\right)}, \quad (\text{A4})$$

where  $r_b$  is the break radius, defined as the location at which the slope of the surface brightness profile changes, and  $I_b$  is the SB at  $r_b$ .

The work of [Baes \(2020\)](#) showed that the Sérsic profile is a unique subgroup of the Nuker function; hence, the de Vaucouleurs profile, the exponential profile, and the Gaussian profile discussed below become specific cases of the Nuker profile, as well.

2. **Sérsic ([Sérsic, 1968](#))**: This profile was introduced as a generalization of the de Vaucouleurs profile and is typically used to fit bulges, bars, and elliptical galaxies by allowing the concentration index  $n$  to vary:

$$I(r) = I_e \exp \left[ -\kappa_n \left( \left( \frac{r}{r_e} \right)^{\frac{1}{n}} - 1 \right) \right], \quad (\text{A5})$$

where  $I_e$  is the SB at the effective radius,  $r_e$ , which encloses half of the luminosity. The parameter  $\kappa_n$  is related to  $n$ , so  $r_e$  becomes the half-light radius; for  $n \in \mathbb{R}$ ,  $\kappa_n = 2n - \frac{1}{3} + \frac{4}{405n} + \frac{46}{25515n^2} + O(n^{-3})$  gives an approximation ([Ciotti & Bertin, 1999](#)). See, for example, GALFIT 3 user’s manual and [Graham & Driver \(2005\)](#) for a full discussion on the properties of the Sérsic profile.

3. **de Vaucouleurs ([de Vaucouleurs, 1948](#))**: A particular case of the Sérsic profile (index  $n = 4$ ,  $\kappa_4 = -7.66925$ ). A general tendency shows that  $n$  grows with galaxy luminosity;

<sup>5</sup>See GALFIT 3 user’s manual, downloadable from <https://users.obs.carnegiescience.edu/peng/work/galfit/galfit.html>

however, at high luminosities the tendency levels off ( $n \rightarrow 4$ ) (e.g., Blanton et al., 2003; López-Cruz et al., 2011; Ríos-López et al., 2025). Thus, as originally found by de Vaucouleurs (1948), this profile historically provided a widely used approximation to the SB profiles of giant ellipticals. However, recent studies advocate using flexible Sérsic indices ( $n$  varying) for more accurate descriptions of elliptical galaxies' diverse structures (Graham & Driver, 2005; Kormendy et al., 2009). This profile has the following expression:

$$I(r) = I_e \exp \left[ -7.66925 \left( 1 - \left( \frac{r}{r_e} \right)^{1/4} \right) \right] \quad (\text{A6})$$

4. **Exponential (Patterson, 1940)**: This popular profile is used to fit the disks of spiral galaxies; it's a particular case of the Sérsic profile with  $n = 1$ :

$$I(r) = I_0 \exp \left( -\frac{r}{r_s} \right), \quad (\text{A7})$$

$I_0$  is the central SB and  $r_s$  is called the scale length, which is related to the effective radius by  $r_e = 1.67835 r_s$  for  $n = 1$ . Freeman (1970) proposed a combination of a de Vaucouleurs bulge and an exponential disk to fit late-type galaxies.

5. **Gaussian profile** is used to fit PSF profiles, the contribution of active galactic nuclei and bars; it's a special case of the Sérsic profile when  $n = 0.5$ . The following equation describes it:

$$I(r) = I_0 \exp \left( \frac{-r^2}{2\sigma^2} \right), \quad (\text{A8})$$

The full width parametrizes the scale at half maximum  $FWHM = 2\sqrt{2 \ln 2} \approx 2.355 \sigma$ , instead of  $r_e$ .

6. **Edge-on disk (van der Kruit & Searle, 1981)**: This profile fits the vertical structure of edge-on spiral galaxies. It results after considering a locally isothermal thin disk (van der Kruit & Searle, 1981):

$$I(r, z) = I_0 \left( \frac{r}{r_s} \right) K_1 \left( \frac{r}{r_s} \right) \text{sech}^2 \left( \frac{z}{z_h} \right), \quad (\text{A9})$$

where  $I_0 = I(0, 0)$  is the central SB,  $r_s$  is the scale length on the disk's major axis,  $z_s$  is the scale height on the  $z$  axis perpendicular to the disk, and  $K_1$  is the modified Bessel function of the second kind.

7. **Ferrers<sup>6</sup>**: This model is named after the triaxial potential introduced by Norman Macleod Ferrers (Ferrers, 1877; Binney & Tremaine, 1987, pp. 61-62). The modified Ferrer profile programmed in GALFIT 3 is given by the following expression:

$$I(r) = I_0 \left[ 1 - \left( \frac{r}{r_{out}} \right)^{(2-\beta)} \right]^\alpha, \quad (\text{A10})$$

which shows an almost flat core and an outer truncation, and whose sharpness of the truncation is set by  $\alpha$ , while the central slope is determined by  $\beta$ ,  $I_0$  is the central SB. This profile is only valid for  $r \leq r_{out}$ , i.e.,  $I(r \geq r_{out}) \equiv 0$ .

This profile has been used to fit bars and lenses; it has eight free parameters. Notwithstanding, a Sérsic profile whose index is  $n < 0.5$  approximates the Ferrers profile; therefore, either profile can be used to model the SB of bars. Besides, the results are indistinguishable (e.g., Kim et al., 2015).

8. **Empirical King (Elson, 1999)**: It is given as follows:

$$I(r) = I_0 \left( 1 - \frac{1}{\psi^{\frac{1}{\alpha}}} \right)^{-\alpha} \left( \frac{1}{\xi^{\frac{1}{\alpha}}} - \frac{1}{\psi^{\frac{1}{\alpha}}} \right)^{\alpha}, \quad (\text{A11})$$

where  $\psi = \left( 1 - \frac{r_t}{r_c} \right)^2$  and  $\xi = \left( 1 - \frac{r}{r_c} \right)^2$ , while the core radius  $r_c$ , the truncation radius  $r_t$ , and the power law index  $\alpha$  are free parameters; however, in the standard modified King profile,  $\alpha = 2$ . This profile fits the SB of globular clusters.

9. **Moffat (Moffat, 1969)** is a profile used to fit PSF profiles or the emission of active nuclei of galaxies. The following equation describes it:

$$I(r) = \frac{I_0}{\left( 1 + \left( \frac{r}{r_d} \right)^2 \right)^n}, \quad (\text{A12})$$

where  $n$  is the concentration index; as for the Gaussian profile, the scale is given by  $FWHM = 2 \left( 2^{\frac{1}{n}} - 1 \right)^{\frac{1}{2}} r_d$ . Nevertheless, the Gaussian profile is more widely used than the Moffat.

10. The user could provide the PSF as an image. However, care should be taken when selecting the stellar image's centroid, intensity, and sampling (see GALFIT 3 user's manual).
11. **The background sky** is modeled as a plane, with an optional gradient applied along the  $x$  and  $y$  directions.
12. **Spiral modes** are used to model the spiral arms or asymmetrical galaxies; see Peng et al. (2010) and GALFIT 3 user's manual for more details.

## B. How to install and run EllipSect

### B.1. Installing EllipSect

EllipSect is implemented in Python 3 for the analysis of GALFIT's outputs and the generation of scientific figures, and is available at <https://github.com/canorve/EllipSect>

#### B.1.1. Quick installation

The quickest way to install EllipSect is just by typing this into the command line:

```
1 pip install ellipse
```

#### B.1.2. Step-by-step installation

The following libraries are required to install EllipSect (v3.4.4) along with Python  $\geq$  v3.8 (Van Rossum & Drake, 2009):

- numpy  $\geq$  v1.20.3 (Harris et al., 2020)
- astropy  $\geq$  v5.1 (Astropy Collaboration et al., 2013; Price-Whelan et al., 2018)
- scipy  $\geq$  v1.5.2 (Virtanen et al., 2020)
- matplotlib  $\geq$  v3.5.2 (Hunter, 2007)
- mgefit  $\geq$  v5.0.13 (Cappellari, 2002)
- sphinx  $\geq$  v3.2.1 (Sphinx developers, 2020)

After installing the libraries, download the latest release from the link shown above, and install it via:

```
1 cd EllipSect
2 pip install .
```

<sup>6</sup>Peng et al. (2010) called it modified Ferrer profile.

or

```
1 cd EllipSect
2 python setup.py install
```

To check that everything is working properly, run the automated tests:

```
1 python -m pytest
```

Although GALFIT is not strictly required, it will require to create the model components and sigma image. Ensure you can call GALFIT from the command prompt. Otherwise, the automated tests will fail.

## B.2. Running EllipSect

**Easy run:** Once installed, run the command `EllipSect` in the same directory that you run GALFIT. The easiest way to run the program is:

```
1 EllipSect GALFIT.01
```

**Note:** EllipSect takes the GALFIT output files (`GALFIT.nn`) where `nn` is the output file number you want to plot.

**More options:** As explained in the paper, EllipSect uses an ellipsoid-based grid to compute the SB. The information of this ellipse is obtained from the GALFIT output file, but if the user wants to provide their ellipse parameters, this is done via:

```
1 EllipSect GALFIT.01 -q 0.5 -pa 80
```

In this last example, an ellipse with a 0.5 axis ratio and position angular of 80 (measured from Y-axis) was used to create the plots.

In case your model contains two or more components, the `comp` (or `cp`) option will plot each component (for an example of this check figure 3):

```
1 EllipSect GALFIT.01 -cp
```

There are many options to change the format of the plots such as: `logx`, `ranx`, `rany`, `pix`, `grid`, `dpi`, `galax`, but if the user prefers to make their plots the option `sabout` will create a file (or files) containing the points of the the SB of the galaxy and model at each radius.

To compute the photometry of the galaxy and model such as `snr`, `BIC`, `AIC`, `absolute Magnitude`, `Luminosity`, `Bumpiness`, `Tidal` and other photometric variables the option `phot` creates a file with the computed variables:

```
1 EllipSect GALFIT.01 --phot
```

EllipSect has the option to compute the sky level to compare with or to provide to GALFIT. As explained above, the program uses two methods to compute it: The gradient method and the random box method. To compute the gradient method:

```
1 EllipSect GALFIT.01 -gsky
```

And to compute using the random box method:

```
1 EllipSect GALFIT.01 -rsky
```

The ring's width and box's size can be modified from their default options.

For more options and to see how to use them, type:

```
1 EllipSect --help
```

### B.2.1. Running EllipSect as a script

If you want to use EllipSect inside your Python script, you can call it in the following way:

```
1 from ellipsect.inout.read import ArgParsing
2 from ellipsect.sectors.sect import SectorsGalfit
3
4 args=['GALFIT.01','--logx','--phot','--noplot']
5 parser_args = ArgParsing(args)
6 photapi = SectorsGalfit(parser_args)
7
8 print("Akaike Criterion: ", photapi.AICrit)
9 print("Bulge to Total: ", photapi.BulgeToTotal)
```

**Code 1.** Example Python Code with EllipSect

A manual and more details can be found in <https://github.com/canorve/EllipSect>

## References

- Añorve, C. 2012, PhD thesis, INAOE
- Akaike, H. 1974, IEEE Transactions on Automatic Control, 19, 716
- Astropy Collaboration, Robitaille, T. P., Tollerud, E. J., et al. 2013, A&A, 558, A33, doi: [10.1051/0004-6361/201322068](https://doi.org/10.1051/0004-6361/201322068)
- Baes, M. 2020, A&A, 634, A109, doi: [10.1051/0004-6361/201937209](https://doi.org/10.1051/0004-6361/201937209)
- Barden, M., Häußler, B., Peng, C. Y., McIntosh, D. H., & Guo, Y. 2012, MNRAS, 422, 449, doi: [10.1111/j.1365-2966.2012.20619.x](https://doi.org/10.1111/j.1365-2966.2012.20619.x)
- Binney, J., & Tremaine, S. 1987, Galactic dynamics
- Blakeslee, J. P., Holden, B. P., Franx, M., et al. 2006, ApJ, 644, 30, doi: [10.1086/503539](https://doi.org/10.1086/503539)
- Blanton, M. R., Hogg, D. W., Bahcall, N. A., et al. 2003, ApJ, 594, 186, doi: [10.1086/375528](https://doi.org/10.1086/375528)
- Cappellari, M. 2002, MNRAS, 333, 400, doi: [10.1046/j.1365-8711.2002.05412.x](https://doi.org/10.1046/j.1365-8711.2002.05412.x)
- Chilingarian, I. V., & Zolotukhin, I. Y. 2012, MNRAS, 419, 1727, doi: [10.1111/j.1365-2966.2011.19837.x](https://doi.org/10.1111/j.1365-2966.2011.19837.x)
- Ciotti, L., & Bertin, G. 1999, A&A, 352, 447, doi: [10.48550/arXiv.astr-ph/9911078](https://doi.org/10.48550/arXiv.astr-ph/9911078)
- de Vaucouleurs, G. 1948, Annales d'Astrophysique, 11, 247
- Duggal, C., O'Dea, C. P., Baum, S. A., et al. 2024, ApJ, 965, 17, doi: [10.3847/1538-4357/ad2513](https://doi.org/10.3847/1538-4357/ad2513)
- Elson, R. A. W. 1999, in Globular Clusters, 209–248
- Ferrers, N. M. 1877, Quart. J. Pure and Appl. Math., 14, 1
- Freeman, K. C. 1970, ApJ, 160, 811, doi: [10.1086/150474](https://doi.org/10.1086/150474)
- Gao, H., & Ho, L. C. 2017, ApJ, 845, 114, doi: [10.3847/1538-4357/aa7da4](https://doi.org/10.3847/1538-4357/aa7da4)
- Garduño, L. E., Zaragoza-Cardiel, J., Lara-López, M. A., et al. 2023, MNRAS, 526, 2479, doi: [10.1093/mnras/stad2690](https://doi.org/10.1093/mnras/stad2690)
- Graham, A. W., & Driver, S. P. 2005, Publ. Astron. Soc. Aust., 22, 118, doi: [10.1071/AS05001](https://doi.org/10.1071/AS05001)
- Harris, C. R., Millman, K. J., van der Walt, S. J., et al. 2020, Nature, 585, 357–362, doi: [10.1038/s41586-020-2649-2](https://doi.org/10.1038/s41586-020-2649-2)
- Häussler, B., McIntosh, D. H., Barden, M., et al. 2007, ApJS, 172, 615, doi: [10.1086/518836](https://doi.org/10.1086/518836)

- Hunter, J. D. 2007, *Computing in Science & Engineering*, 9, 90, doi: [10.1109/MCSE.2007.55](https://doi.org/10.1109/MCSE.2007.55)
- Jedrzejewski, R. I. 1987, *MNRAS*, 226, 747, doi: [10.1093/mnras/226.4.747](https://doi.org/10.1093/mnras/226.4.747)
- Kim, T., Sheth, K., Gadotti, D. A., et al. 2015, *ApJ*, 799, 99, doi: [10.1088/0004-637X/799/1/99](https://doi.org/10.1088/0004-637X/799/1/99)
- Kormendy, J., Fisher, D. B., Cornell, M. E., & Bender, R. 2009, *ApJS*, 182, 216, doi: [10.1088/0067-0049/182/1/216](https://doi.org/10.1088/0067-0049/182/1/216)
- Kron, R. G. 1980, *ApJS*, 43, 305, doi: [10.1086/190669](https://doi.org/10.1086/190669)
- Lauer, T. R., Ajhar, E. A., Byun, Y. I., et al. 1995, *AJ*, 110, 2622, doi: [10.1086/117719](https://doi.org/10.1086/117719)
- López-Cruz, O. 1997, PhD thesis, University of Toronto, Canada
- López-Cruz, O., Añorve, C., Birkinshaw, M., et al. 2014, *ApJ*, 795, L31, doi: [10.1088/2041-8205/795/2/L31](https://doi.org/10.1088/2041-8205/795/2/L31)
- López-Cruz, O., Aguilar, L. A., & Añorve, C. 2011, in *Revista Mexicana de Astronomía y Astrofísica Conference Series*, Vol. 39, 100–108
- López-Cruz, O., Barkhouse, W. A., & Yee, H. K. C. 2004, *ApJ*, 614, 679, doi: [10.1086/423664](https://doi.org/10.1086/423664)
- Lucy, L. B. 1974, *AJ*, 79, 745, doi: [10.1086/111605](https://doi.org/10.1086/111605)
- Moffat, A. F. J. 1969, *A&A*, 3, 455
- Patterson, F. S. 1940, *Harvard College Observatory Bulletin*, 914, 9
- Peng, C. Y., Ho, L. C., Impey, C. D., & Rix, H.-W. 2002, *AJ*, 124, 266, doi: [10.1086/340952](https://doi.org/10.1086/340952)
- , 2010, *AJ*, 139, 2097, doi: [10.1088/0004-6256/139/6/2097](https://doi.org/10.1088/0004-6256/139/6/2097)
- Petrosian, V. 1976, *ApJ*, 209, L1, doi: [10.1086/182253](https://doi.org/10.1086/182253)
- Press, W. H., Teukolsky, S. A., Vetterling, W. T., & Flannery, B. P. 2007, in *Numerical Recipes: The Art of Scientific Computing*, 3rd edn. (New York: Cambridge University Press), 800–804
- Price-Whelan, A. M., Sipőcz, B. M., Günther, H. M., et al. 2018, *AJ*, 156, 123, doi: [10.3847/1538-3881/aabc4f](https://doi.org/10.3847/1538-3881/aabc4f)
- Reyes-Amador, C. 2021, Master's thesis, Instituto de Radioastronomía y Astrofísica
- Richardson, W. H. 1972, *J. Opt. Soc. Am.*, 62, 55, doi: [10.1364/JO SA.62.000055](https://doi.org/10.1364/JO SA.62.000055)
- Ríos-López, E. 2021, PhD thesis, INAOE
- Ríos-López, E., Añorve, C., Ibarra-Medel, H. J., et al. 2021, *MNRAS*, 507, 5952, doi: [10.1093/mnras/stab2321](https://doi.org/10.1093/mnras/stab2321)
- Ríos-López, E., López-Cruz, O., Añorve, C., et al. 2025, arXiv e-prints, arXiv:2502.02546, doi: [10.48550/arXiv.2502.02546](https://doi.org/10.48550/arXiv.2502.02546)
- Ríos-López, E., López-Cruz, O., Añorve, C., et al. 2025, *Monthly Notices of the Royal Astronomical Society*, 539, 2583, doi: [10.1093/mnras/staf606](https://doi.org/10.1093/mnras/staf606)
- Schlafly, E. F., & Finkbeiner, D. P. 2011, *ApJ*, 737, 103, doi: [10.1088/0004-637X/737/2/103](https://doi.org/10.1088/0004-637X/737/2/103)
- Schwarz, G. 1978, *Annals of Statistics*, 6, 461
- Sérsic, J. L. 1968, *Atlas de Galaxias Australes*
- Sphinx developers. 2020, Sphinx: Python documentation generator, <https://pypi.org/project/Sphinx/3.2.1/>
- Tal, T., van Dokkum, P. G., Nelan, J., & Bezanson, R. 2009, *AJ*, 138, 1417, doi: [10.1088/0004-6256/138/5/1417](https://doi.org/10.1088/0004-6256/138/5/1417)
- van der Kruit, P. C., & Searle, L. 1981, *A&A*, 95, 105
- Van Rossum, G., & Drake, F. L. 2009, *Python 3 Reference Manual* (Scotts Valley, CA: CreateSpace)
- Virtanen, P., Gommers, R., Oliphant, T. E., et al. 2020, *Nature Methods*, 17, 261, doi: [10.1038/s41592-019-0686-2](https://doi.org/10.1038/s41592-019-0686-2)
- Willmer, C. N. A. 2018, *ApJS*, 236, 47, doi: [10.3847/1538-4365/aabfdf](https://doi.org/10.3847/1538-4365/aabfdf)